

Magnetic transition behavior and large topological Hall effect in hexagonal $\text{Mn}_{2-x}\text{Fe}_{1+x}\text{Sn}$ ($x = 0.1$) magnet

Cite as: Appl. Phys. Lett. **117**, 052407 (2020); <https://doi.org/10.1063/5.0011570>
 Submitted: 22 April 2020 . Accepted: 24 July 2020 . Published Online: 07 August 2020

Jun Liu,  Shulan Zuo,  Xinqi Zheng,  Ying Zhang, Tongyun Zhao,  Fengxia Hu,  Jirong Sun, and  Baogen Shen



View Online



Export Citation



CrossMark

ARTICLES YOU MAY BE INTERESTED IN

[Size-dependent anomalous Hall effect in noncollinear antiferromagnetic \$\text{Mn}_3\text{Sn}\$ films](#)

Applied Physics Letters **117**, 052404 (2020); <https://doi.org/10.1063/5.0011566>

[Large topological Hall effect in an easy-cone ferromagnet \$\(\text{Cr}_{0.9}\text{B}_{0.1}\)\text{Te}\$](#)

Applied Physics Letters **117**, 052409 (2020); <https://doi.org/10.1063/5.0018229>

[Current-induced bulk magnetization of a chiral crystal \$\text{CrNb}_3\text{S}_6\$](#)

Applied Physics Letters **117**, 052408 (2020); <https://doi.org/10.1063/5.0017882>



Your Qubits. Measured.

Meet the next generation of quantum analyzers

- Readout for up to 64 qubits
- Operation at up to 8.5 GHz, mixer-calibration-free
- Signal optimization with minimal latency

Find out more



Magnetic transition behavior and large topological Hall effect in hexagonal $\text{Mn}_{2-x}\text{Fe}_{1+x}\text{Sn}$ ($x = 0.1$) magnet

Cite as: Appl. Phys. Lett. **117**, 052407 (2020); doi: 10.1063/5.0011570

Submitted: 22 April 2020 · Accepted: 24 July 2020 ·

Published Online: 7 August 2020



View Online



Export Citation



CrossMark

Jun Liu,^{1,2} Shulan Zuo,³ Xinqi Zheng,⁴ Ying Zhang,¹ Tongyun Zhao,¹ Fengxia Hu,^{1,2} Jirong Sun,^{1,2} and Baogen Shen^{1,2,a)}

AFFILIATIONS

¹State Key Laboratory of Magnetism, Institute of Physics, Chinese Academy of Sciences, Beijing 100190, People's Republic of China

²University of Chinese Academy of Sciences, Beijing 100049, People's Republic of China

³School of Materials Science and Engineering, Beihang University, Beijing 100191, People's Republic of China

⁴School of Materials Science and Engineering, University of Science and Technology Beijing, Beijing 100083, People's Republic of China

^{a)} Author to whom correspondence should be addressed: shenbaogen@yeah.net

ABSTRACT

The magnetic transition, transport properties, and magnetic domain structures of the polycrystalline $\text{Mn}_{1.9}\text{Fe}_{1.1}\text{Sn}$ compound with a hexagonal structure have been investigated. The result shows that ferromagnetic and antiferromagnetic phases coexist in this compound. A large topological Hall effect up to $3.5 \mu\Omega\cdot\text{cm}$ at 50 K has been found due to the formation of noncoplanar spin structures when the competition occurs among magnetocrystalline anisotropy, antiferromagnetic coupling, and ferromagnetic interaction at low temperature. The result of *in situ* Lorentz transmission electron microscopy cooling experiment at zero field indicates two shapes of domain walls containing vortexes coexisting simultaneously in the compound.

Published under license by AIP Publishing. <https://doi.org/10.1063/5.0011570>

Heusler compounds have always been the focus of attention due to their fascinating physical properties and potential applications in spintronics,^{1–3} half-metals,^{4,5} ferromagnetic shape memory alloys,^{6–8} and magnetocaloric effects.^{9,10} A classic composition is defined as the X_2YZ structure, where X and Y are transition or rare-earth metals and Z is a main group element. Generally, they crystallize a kind of cubic structure such as the Cu_2MnAl -type Heusler structure (space group Fm-3m) or Li_2AgSb -type so-called inverse Heusler structure (space group F-43m). If its crystal structure is compressed or stretched by external conditions along cubic $\langle 001 \rangle$ or $\langle 111 \rangle$ axes, the tetragonal or hexagonal lattice can also be generated, respectively.¹¹ As a result, other crystal configurations can be found in previous literature.^{12,13}

The important one among them is Mn_2 -based Heusler alloys, which have received widespread attention recently. Gasi *et al.* reported the exchange-spring magnetic behavior in Mn_2FeGa alloy.¹⁴ Liu *et al.* also found the giant exchange bias up to 0.132 T at 5 K in this alloy.¹³ Luo *et al.* predicted theoretically that Mn_2FeZ Heusler compounds would present the half-metallic feature for $Z=\text{Al}$ and Sb .¹⁵ Faleev *et al.*

predicted that Mn_2FeSn is an inverse Heusler alloy of tetragonal distortion by the peak-and-valley feature of the density of states (DOS).¹⁶ Ma *et al.* thought that Mn_2FeSn will have a pseudogap after 9 states in majority, which can generate a half-metal or near-half-metal by theoretical calculations.¹⁷ At the same time, the large topological Hall effect was reported in Mn_2PtSn bulk and thin films.^{12,18} Those characteristics motivate one to find other Mn_2 -based alloys and have a comprehensive research. In addition, Fichtner *et al.* reported that some parameters such as magnetic moment, Curie temperature, Seebeck coefficient, and electrical properties can be regulated by variation of the Mn content in the $\text{Ni}_{2-x}\text{Mn}_{1+x}\text{Sn}$ alloys.¹⁹ Giant exchange bias can also be attained by the adjustment of the Mn/Fe ratio in $\text{Mn}_{2-x}\text{Fe}_{1+x}\text{Ga}$ with $x = 0.3$ and 0.5 .²⁰ Interestingly, off-stoichiometric Ni–Mn–Ga alloys exhibited the rich magnetic domain structures, such as magnetic bubbles and biskyrmions.^{21–23} Until now, however, there are few research studies on $\text{Mn}_{2-x}\text{Fe}_{1+x}\text{Sn}$ alloys in experimental details. Chemical order and the coexistence of multiple phases add the mysterious and complex features for Mn_2 -based Heusler alloys.^{13,24} Felez *et al.* studied the tunable Curie temperature by substituting Fe

for Mn in the Mn_3Sn compound.²⁵ The result shows that the $\text{Mn}_{3-x}\text{Fe}_x\text{Sn}$ ($x = 1$) alloy displays a typical ferromagnetic feature and has a Curie temperature that is near or higher than room temperature, which is beneficial for the observation of the magnetic domain structure. Based on these reasons, $\text{Mn}_{2-x}\text{Fe}_{1+x}\text{Sn}$ alloys with $x = 0.1$ were selected to be studied in detail. The crystalline structure, magnetic transition, magneto-transport properties, and magnetic domain structure of this alloy were investigated. It was found that the alloy exhibits a large topological Hall effect at low temperature and an interesting magnetic domain structure.

A high quality polycrystalline $\text{Mn}_{1.9}\text{Fe}_{1.1}\text{Sn}$ ingot was prepared by the traditional arc-melting method under protection of a high-purity argon atmosphere. The phase component and the crystalline structure were characterized by the x-ray diffraction (XRD) measurement using a Rigaku D/Max-2400 diffractometer with $\text{Cu K}\alpha$ radiation ($\lambda = 1.541 \text{ \AA}$). The thin plate for Lorentz transmission electron microscopy (LTEM) observation was prepared by traditional mechanical polishing and argon ion milling. A JEOL-dedicated LTEM was used to image the magnetic domain configuration with almost no remnant magnetic field near the sample. A liquid-nitrogen TEM sample holder (from room temperature to about 100 K) was employed to perform an *in situ* cooling experiment. Magnetic properties were examined using a superconducting quantum interference device magnetometer (SQUID-VSM). Transport properties were measured on a Quantum Design Physical Property Measurement System (PPMS).

The typical powder XRD pattern and Rietveld refined result at room temperature of the $\text{Mn}_{1.9}\text{Fe}_{1.1}\text{Sn}$ alloy are displayed in Fig. 1(a). All the diffraction peaks of the sample can be indexed as the D0_{19} type hexagonal structure with space group $\text{P6}_3/\text{mmc}$ rather than the conventional cubic structure. The lattice parameters from the result of Rietveld refined are $a = 0.5567 \text{ nm}$ and $c = 0.4449 \text{ nm}$. It should be stressed that the strongest peak in Mn_2FeGa with the same crystal structure is the (201) peak rather than the (002) peak,¹³ which

indicates a strong texture along the [002] crystal orientation in the prepared sample. The result of the x-ray energy dispersive spectrometer (EDS) shows that the average atomic ratio of $\text{Mn}:\text{Fe}:\text{Sn}$ is about 0.4727:0.2448:0.2825, which is close to the stoichiometric ratio of $\text{Mn}_{1.9}\text{Fe}_{1.1}\text{Sn}$. Figure 1(b) shows the temperature dependence of magnetization of the sample. Zero-field-cooled (ZFC) and field-cooled (FC) magnetization vs temperature (M - T) curves were recorded at temperatures from 5 K to 380 K under an applied field of 0.01 T. As it can be seen from Fig. 1(b), the magnetization slightly decreases upon increasing temperature from 5 K to 128 K (T_I), manifesting that the alloy first undergoes a process of spin reorientation due to rotation of magnetic moments. When the temperature increases to 171 K (T_N), there are two cusps in both ZFC and FC curves, indicating that a magnetic transition occurs from antiferromagnetism (AFM) to paramagnetism (PM) for one phase in the alloy. The magnetization sharply reduces at 323 K (T_C) upon further increasing the temperature, which shows a ferromagnetic (FM) transition for another phase. According to the previous result,²⁶ the coexistence of FM and AFM phases is not uncommon in the polycrystalline Mn-Fe-Sn system, which is also found in our sample. Moreover, we make a fit of the high-temperature zone where the reciprocal of susceptibility presents a good linear behavior, indicating that the paramagnetic Curie temperature θ_p of $\text{Mn}_{1.9}\text{Fe}_{1.1}\text{Sn}$ alloy is about 330 K [inset of Fig. 1(b)].

Figure 1(c) exhibits the magnetic hysteresis loops measured with applied fields up to 5 T at various temperatures. All magnetization curves exhibit the character of FM, namely, the magnetization rapidly rises with the increasing magnetic field. An obvious hysteresis has been found in the magnetization curve at 50 K, and the coercivity decreases from 0.34 T at 50 K to 0 T at 130 K (slightly higher than T_I), which is due to the change of magnetocrystalline anisotropy with the increase in temperature.²⁷ It should be pointed out that the magnetization shows a linear magnetization process under a low field below 170 K, which is regarded as the feature of AFM.²⁸ In addition, this “collapse” phenomenon in magnetization curves was thought as decoupling interaction in permanent or nanocomposite materials due to the weak exchange-coupling between two magnetic phases.^{29,30} This evidence favors a conclusion that the sample is the coexistence of FM and FM in the low-temperature zone, which is in accord with the analysis in M - T curves above. When the temperature is higher than 180 K, the sample presents a standard feature of soft magnetic materials.

Transport properties are measured by a standard six-electrode method. Figure 1(d) shows the temperature dependence of longitudinal resistivity ρ ranging from 5 K to 300 K under zero magnetic field. It can be obviously seen that ρ drops mildly from $300 \mu\Omega\cdot\text{cm}$ at 5 K to $263 \mu\Omega\cdot\text{cm}$ at 300 K, presenting a negative temperature coefficient (NTC). In pursuance of the empirical rule of Mooij, metallic materials with electrical resistivity values above $100\text{--}200 \mu\Omega\cdot\text{cm}$ usually show a NTC for all temperatures.^{31–33} It reveals that the sample exhibits the nonmetallic behavior. A similar phenomenon has also been observed in $\text{Ni}_{2-x}\text{Mn}_{1+x}\text{Sn}$ alloy with $x = 1$ and $\text{Sr}_2\text{FeMoO}_6$.^{19,34} Fichtner *et al.* thought that this situation is caused by chemical disorder. When the metal acquires its critical disorder value (Ioffe-Regel limit), the increase in disorder results in the efficient electron screening of the scattering potentials.¹⁹ Kobayashi *et al.* attribute the phenomenon to the preparation procedures of samples in the ceramic of $\text{Sr}_2\text{FeMoO}_6$.³⁴ However, we speculate that it is likely to the change in

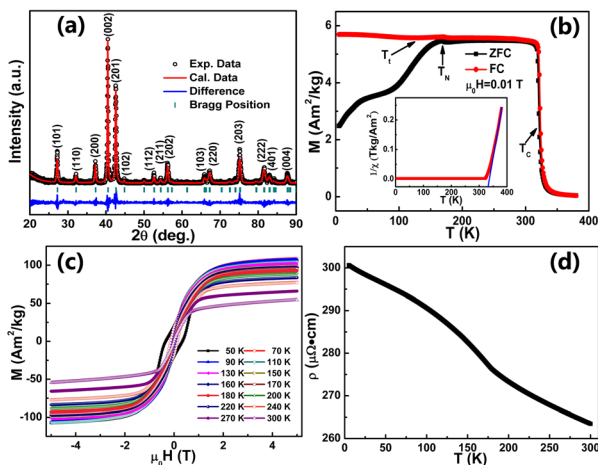


FIG. 1. (a) XRD patterns and Rietveld refined results of the $\text{Mn}_{1.9}\text{Fe}_{1.1}\text{Sn}$ compound measured at room temperature. (b) Temperature dependence of ZFC and FC magnetization under a magnetic field of 0.01 T. The inset shows the temperature dependence of the inverse susceptibility χ^{-1} . (c) Hysteresis loops sweeping field between 5 T and -5 T at different temperatures from 50 K to 300 K. (d) Temperature dependence of longitudinal resistivity under zero field.

the band structure for $\text{Mn}_{2-x}\text{Fe}_{1+x}\text{Sn}$ alloy, presenting a half-metallic conductivity.^{17,35}

The magnetic field dependence of Hall resistivity ρ_{xy} under the same measurement condition is displayed in Fig. 2(a). The ρ_{xy} -H curves also show the hysteresis effect below 130 K similar to the hysteresis loops [Fig. 1(c)]. The value of ρ_{xy} decreases with the increase in temperature, which coincides with the trend of the ρ -T curve above. Generally, Hall resistivity ρ_{xy} can be expressed as $\rho_{xy} = \rho_{xy}^N + \rho_{xy}^A + \rho_{xy}^T = R_0B + S_A\rho_{xx}^2M + \rho_{xy}^T$, where normal Hall resistivity ρ_{xy}^N has a linear relationship with applied magnetic field B. Anomalous Hall resistivity ρ_{xy}^A is proportional to the magnetization. Topological Hall resistivity ρ_{xy}^T will disappear under high magnetic fields due to the full aligned arrangement of magnetic moments. R_0 is the normal Hall coefficient, and S_A stands for the scaling coefficient independent of field B.^{36,37} According to the ρ_{xy} -H curves of the sample, it can be clearly observed that ρ_{xy} contains both normal Hall resistivity ρ_{xy}^N and anomalous Hall resistivity ρ_{xy}^A . Therefore, the formula $\rho_{xy}/B = R_0 + S_A\rho_{xx}M/B$ is employed to fit the constant R_0 and S_A at the fixed temperature where the value of R_0 and S_A can be obtained from the intercept and slope of the linear curve, respectively, as shown in Fig. 2(b). The value of R_0 changes the sign from negative to positive at 180 K, demonstrating that the type of conduction transforms from electrons to holes. A previous report also shows the change in the charge carrier type in the ribbon of Mn_2PtSn due to the competition between two conducting charge carriers.¹⁸ In addition, it cannot be ruled out that the change in the magnetic structure results in the alteration of the band structure around 180 K. Hence, the precise electronic and magnetic structures need to be studied further.

Topological Hall resistivity ρ_{xy}^T is obtained by subtracting ρ_{xy}^N and ρ_{xy}^A from total ρ_{xy} , as plotted in Fig. 2(c). A large ρ_{xy}^T about near $3.5 \mu\Omega\text{-cm}$ is found in the sample at 50 K, which is slightly larger than the maximum value at 2 K of Mn_3Sn .²⁷ Then, it damps promptly to

$0.18 \mu\Omega\text{-cm}$ at 170 K. When the temperature rises to 180 K, the sign of ρ_{xy}^T changes from positive to negative. We think that the topological Hall effect is attributed to the competition among magnetocrystalline anisotropy, antiferromagnetic coupling, and ferromagnetic interaction. This may be explained as follows: when the temperature is lower than 130 K (near T_I), the competition among three factors together influences the magnetic texture of the $\text{Mn}_{1.9}\text{Fe}_{1.1}\text{Sn}$ alloy. In general, antiferromagnetic coupling and ferromagnetic interaction make magnetic moments tend to collinear arrangement in the c-plane for the $\text{Mn}_{1.9}\text{Fe}_{1.1}\text{Sn}$ alloy. But magnetocrystalline anisotropy on account of strong texture along the c-axis causes the rotation of magnetic moments from the c-plane toward the c-axis, further resulting in the formation of noncoplanar spin structures. It can induce the Berry phase to the conduction electrons, which will contribute to the Hall resistivity.^{38,39} The stronger the anisotropy is, the greater the angle of deviation is. Upon increasing the temperature to 180 K (near T_N), the abatement of anisotropy gradually weakens the competition with two other factors, thus leading to the reduction of ρ_{xy}^T . When the temperature exceeds 180 K further, only the weak anisotropy and ferromagnetic interaction take part in the competition to the formation noncoplanar spin textures as a result of AFM phase transition, producing the lower level of ρ_{xy}^T . At the same time, the alteration of the sign of ρ_{xy}^T at 180 K is likely due to the same reason.

To roughly illustrate the temperature dependence of magnetocrystalline anisotropy constant K_u , we determine the anisotropy field H_k at different temperatures referring to the literature.⁴⁰ The formula $K_u = H_k M_s / 2$ is employed to calculate the value of K_u , shown in Fig. 2(d), where the saturation magnetization M_s is determined by the law of approach to saturation (LATS).⁴¹ A monotonically decreasing trend for the value of K_u can be found with increasing temperature, and there is a faster rate of decent at low temperature. It demonstrates the rapid change of magnetocrystalline anisotropy with the increase in temperature, which have a strongly effect on the domain. This appearance of the topological Hall effect may also indicate the appearance of diversifying domain structures over a very wide temperature region.

Figure 3 displays the under-focused LTEM images of the temperature dependence of magnetic domain evolution for the $\text{Mn}_{1.9}\text{Fe}_{1.1}\text{Sn}$ alloy at selected temperatures. A series of vortices and anti-vortices can be seen in Fig. 3(a) at 273 K (below T_C). It should be noted that there are two shapes of domain walls of vortices. One, marked with I and II in Figs. 3(b) and 3(c), is the so-called one-dimensional periodic array composed of the alternating “dark dots” (bright dots) and “bright lines” (dark lines), which is elaborated in the supplementary material of $\text{La}_{1-x}\text{Sr}_x\text{MnO}_3$ with $x = 0.175$ at length.⁴² Another is the cross-tie domain wall marked III in Figs. 3(b) and 3(c), which consists of the alternate vortex and antivortex and has been thoroughly studied in the amorphous Ce-Fe-B system.⁴³ With the decrease in temperature, the vortices begin to annihilate [Figs. 3(b)–3(e)]. When temperature decreases to 178 K below [Figs. 3(f)–3(i)], the pairs of vortex and anti-vortex totally vanish and the domain walls transform into the conventional Bloch walls. According to the analysis of magnetic anisotropy constant K_u , it shows a low value when temperature is higher than 200 K. A large number of vortices are likely to be related to the low magnetocrystalline anisotropy of the sample in this temperature region,⁴⁴ which is consistent with the afore-mentioned analysis.

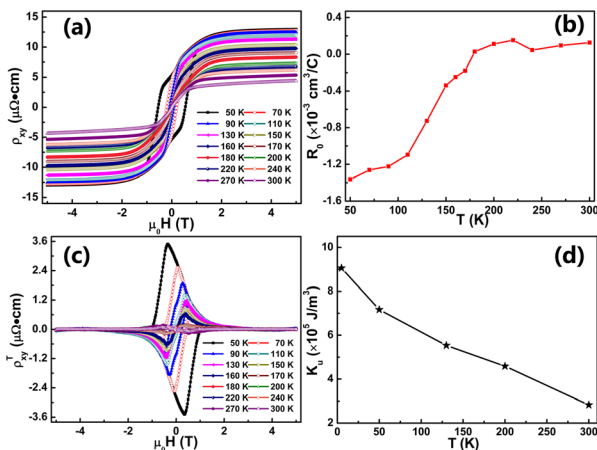


FIG. 2. (a) Hall resistivities ρ_{xy} as a function at various temperatures ranging from 50 K to 300 K for the $\text{Mn}_{1.9}\text{Fe}_{1.1}\text{Sn}$ compound. (b) Temperature dependence of ordinary Hall coefficient R_0 obtained by fitting the formula. (c) Magnetic field dependence of ρ_{xy}^T extracting from total ρ_{xy} in the same temperature region. (d) Temperature dependence of the magnetocrystalline anisotropy constant (K_u) ranging from 5 K to 300 K.

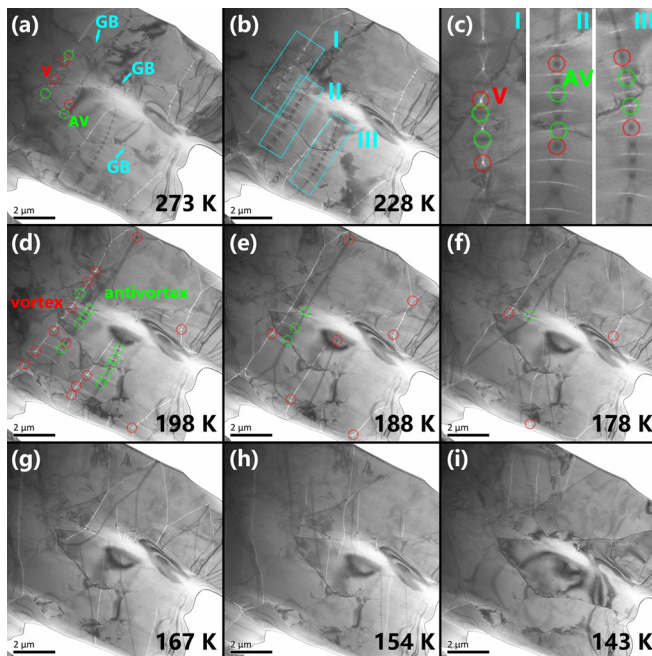


FIG. 3. Magnetic domain structure evolution observed by means of LTEM in under-focus mode for the $\text{Mn}_{1.9}\text{Fe}_{1.1}\text{Sn}$ thin plate as the temperature was decreased from 273 K to 143 K at zero magnetic field. (a) 273 K, (b) 228 K, (d) 198 K, (e) 188 K, (f) 178 K, (g) 167 K, (h) 154 K, and (i) 143 K. (c) The magnified images for three selected areas of (b). Vortex (V) and antivortex (AV) are marked by red and green circles in Figs. 3(a)–3(f), respectively.

Unfortunately, the magnetic domain structure cannot be detected below 128 K (T_c) owing to the technical limitation of the current measurement, but we can predict that an interesting domain structure may exist in $\text{Mn}_{1.9}\text{Fe}_{1.1}\text{Sn}$ alloy in the lower temperature zone as a result of the appearance of the topological Hall effect at zero field.

In conclusion, we reported the magnetization, transport properties, and magnetic domains of the polycrystalline $\text{Mn}_{1.9}\text{Fe}_{1.1}\text{Sn}$ compound. A large topological Hall effect up to $3.5 \mu\Omega\cdot\text{cm}$ at 50 K has been found due to the formation of the noncoplanar spin structure when the competition among magnetocrystalline anisotropy, antiferromagnetic coupling, and ferromagnetic interaction occurs at low temperature. The result of *in situ* Lorentz transmission electron microscopy cooling experiment at zero field indicates two shapes of domain walls including vortices and antivortices that coexist in this sample.

See the [supplementary material](#) for the composition (S1), the magnified view of hysteresis loops at different temperatures (S2), extraction of topological Hall resistivity at representative temperature (S3), the fitting value of scaling coefficient S_A (S4), the field dependence of magnetization of the hard-axis (black line) and easy-axis (red line) in the wide temperature range and temperature dependence of the saturation magnetization M_s (S5), and the experimental results of hysteresis loops and Hall resistivity of the repeated sample (S6).

This work was supported by the National Key Research and Development Program of China (Grant Nos. 2016YFB0700903,

2017YFA0206300, and 2016YFA0300701), the National Natural Science Foundation of China (Grant Nos. 51590881 and 11520101002), and the Key Program of the Chinese Academy of Sciences of China (Grant Nos. QYZDY-SSW-SLH020 and 112111KYSB20180013).

DATA AVAILABILITY

The data that support the findings of this study are available within this article and its [supplementary material](#).

REFERENCES

- T. Jungwirth, X. Marti, P. Wadley, and J. Wunderlich, *Nat. Nanotechnol.* **11**, 231 (2016).
- K. Yakushiji, K. Saito, S. Mitani, K. Takanashi, Y. K. Takahashi, and K. Hono, *Appl. Phys. Lett.* **88**, 222504 (2006).
- C. Felser, G. H. Fecher, and B. Balke, *Angew. Chem., Int. Ed.* **46**, 668 (2007).
- R. Weht and W. E. Pickett, *Phys. Rev. B* **60**, 13006 (1999).
- G. D. Liu, X. F. Dai, H. Y. Liu, J. L. Chen, Y. X. Li, G. Xiao, and G. H. Wu, *Phys. Rev. B* **77**, 014424 (2008).
- I. Takeuchi, O. O. Famodu, J. C. Read, M. A. Aronova, K.-S. Chang, C. Craciunescu, S. E. Lofland, M. Wuttig, F. C. Wellstood, L. Knauss, and A. Orozco, *Nat. Mater.* **2**, 180 (2003).
- Y. Sutou, Y. Imano, N. Koeda, T. Omori, R. Kainuma, K. Ishida, and K. Oikawa, *Appl. Phys. Lett.* **85**, 4358 (2004).
- H. E. Karaca, I. Karaman, B. Basaran, D. C. Lagoudas, Y. I. Chumlyakov, and H. J. Maier, *Acta Mater.* **55**, 4253 (2007).
- P. J. Shamberger and F. S. Ohuchi, *Phys. Rev. B* **79**, 144407 (2009).
- A. Planes, L. Mañosa, and M. Acet, *J. Phys.: Condens. Matter* **21**, 233201 (2009).
- K. Manna, Y. Sun, L. Muechler, J. Kubler, and C. Felser, *Nat. Rev. Mater.* **3**, 244 (2018).
- Y. Q. Li, B. Ding, X. T. Wang, H. W. Zhang, W. H. Wang, and Z. Y. Liu, *Appl. Phys. Lett.* **113**, 062406 (2018).
- Z. H. Liu, Y. J. Zhang, H. G. Zhang, X. J. Zhang, and X. Q. Ma, *Appl. Phys. Lett.* **109**, 032408 (2016).
- T. Gasi, A. K. Nayak, J. Winterlik, V. Ksenofontov, P. Adler, M. Nicklas, and C. Felser, *Appl. Phys. Lett.* **102**, 202402 (2013).
- H. Z. Luo, H. W. Zhang, Z. Y. Zhu, L. Ma, S. F. Xu, G. H. Wu, X. X. Zhu, C. B. Jiang, and H. B. Xu, *J. Appl. Phys.* **103**, 083908 (2008).
- S. V. Faleev, Y. Ferrante, J. Jeong, M. G. Samant, B. Jones, and S. S. P. Parkin, *Phys. Rev. Appl.* **7**, 034022 (2017).
- J. H. Ma, J. G. He, D. Mazumdar, K. Munira, S. Keshavarz, T. Lovorn, C. Wolverton, A. W. Ghosh, and W. Butler, *Phys. Rev. B* **98**, 094410 (2018).
- Z. H. Liu, A. Burigu, Y. J. Zhang, H. M. Jafri, X. Q. Ma, E. K. Liu, W. H. Wang, and G. H. Wu, *Scr. Mater.* **143**, 122 (2018).
- T. Fichtner, G. Kreiner, S. Chadov, G. H. Fecher, W. Schnelle, A. Hoser, and C. Felser, *Intermetallics* **57**, 101 (2015).
- A. K. Nayak, M. Nicklas, S. Chadov, P. Khuntia, C. Shekhar, A. Kalache, M. Baenitz, Y. Skourski, V. K. Guduru, A. Puri, U. Zeitler, J. M. D. Coey, and C. Felser, *Nat. Mater.* **14**, 679 (2015).
- S. L. Zuo, Y. Zhang, L. C. Peng, X. Zhao, R. Li, H. Li, J. F. Xiong, M. He, T. Y. Zhao, J. R. Sun, F. X. Hu, and B. G. Shen, *Nanoscale* **10**, 2260 (2018).
- B. Ding, H. Li, X. Y. Li, Y. Wang, Z. P. Hou, G. Z. Xu, E. K. Liu, G. H. Wu, F. W. Wang, and W. H. Wang, *APL Mater.* **6**, 076101 (2018).
- B. Ding, J. Cui, G. Z. Xu, Z. P. Hou, H. Li, E. K. Liu, G. H. Wu, Y. Yao, and W. H. Wang, *Phys. Rev. Appl.* **12**, 054060 (2019).
- L. Ma, W. H. Wang, J. B. Lu, J. Q. Li, C. M. Zhen, D. L. Hou, and G. H. Wu, *Appl. Phys. Lett.* **99**, 182507 (2011).
- M. R. Felez, A. A. Coelho, and S. Gama, *J. Magn. Magn. Mater.* **444**, 280 (2017).
- T. Hori, H. Niida, Y. Yamaguchi, H. Kato, and Y. Nakagawa, *J. Magn. Magn. Mater.* **90–91**, 159 (1990).
- P. K. Rout, P. V. P. Madduri, S. K. Manna, and A. K. Nayak, *Phys. Rev. B* **99**, 094430 (2019).
- X. Q. Zheng, X. P. Shao, J. Chen, Z. Y. Xu, F. X. Hu, J. R. Sun, and B. G. Shen, *Appl. Phys. Lett.* **102**, 022421 (2013).
- D. Goll, M. Seeger, and H. Kronmüller, *J. Magn. Magn. Mater.* **185**, 49 (1998).

- ³⁰J. P. Liu, R. Skomski, Y. Liu, and D. J. Sellmyer, *J. Appl. Phys.* **87**, 6740 (2000).
- ³¹N. E. Hussey, K. Takenaka, and H. Takagi, *Philos. Mag.* **84**, 2847 (2004).
- ³²J. H. Mooij, *Phys. Status Solidi A* **17**, 521 (1973).
- ³³I. Gavrikov, M. Seredina, M. Zheleznyy, I. Shchetinin, D. Karpenkov, A. Bogach, R. Chatterjee, and V. Khovaylo, *J. Magn. Magn. Mater.* **478**, 55 (2019).
- ³⁴K.-I. Kobayashi, T. Kimura, H. Sawada, K. Terakura, and Y. Tokura, *Nature* **395**, 677 (1998).
- ³⁵X. Wang, M. Liu, X. D. Shen, Z. H. Liu, Z. W. Hu, K. Chen, P. Ohresser, L. Nataf, F. Baudalet, H.-J. Lin, C.-T. Chen, Y.-L. Soo, Y. F. Yang, C. Q. Jin, and Y. W. Long, *Inorg. Chem.* **58**, 320 (2019).
- ³⁶M. Lee, Y. Onose, Y. Tokura, and N. P. Ong, *Phys. Rev. B* **75**, 172403 (2007).
- ³⁷N. Kanazawa, Y. Onose, T. Arima, D. Okuyama, K. Ohoyama, S. Wakimoto, K. Kakurai, S. Ishiwata, and Y. Tokura, *Phys. Rev. Lett.* **106**, 156603 (2011).
- ³⁸N. Nagaosa, J. Sinova, S. Onoda, A. H. MacDonald, and N. P. Ong, *Rev. Mod. Phys.* **82**, 1539 (2010).
- ³⁹H. Li, B. Ding, J. Chen, Z. F. Li, Z. P. Hou, E. K. Liu, H. W. Zhang, X. K. Xi, G. H. Wu, and W. H. Wang, *Appl. Phys. Lett.* **114**, 192408 (2019).
- ⁴⁰Z. P. Hou, W. J. Ren, B. Ding, G. Z. Xu, Y. Wang, B. Yang, Q. Zhang, Y. Zhang, E. K. Liu, F. Xu, W. H. Wang, G. H. Wu, X. X. Zhang, B. G. Shen, and Z. D. Zhang, *Adv. Mater.* **29**, 1701144 (2017).
- ⁴¹S. V. Andreev, M. I. Bartashevich, V. I. Pushkarsky, V. N. Maltsev, L. A. Pamyatnykh, E. N. Tarasov, N. V. Kudrevatykh, and T. Goto, *J. Alloys Compd.* **260**, 196 (1997).
- ⁴²X. Z. Yu, Y. Tokunaga, Y. Taguchi, and Y. Tokura, *Adv. Mater.* **29**, 1603958 (2017).
- ⁴³S. L. Zuo, M. Zhang, R. Li, Y. Zhang, L. C. Peng, J. F. Xiong, D. Liu, T. Y. Zhao, F. X. Hu, B. G. Shen, and J. R. Sun, *Acta Mater.* **140**, 465 (2017).
- ⁴⁴S. P. Venkateswaran, N. T. Nuhfer, and M. D. Graef, *Acta Mater.* **55**, 2621 (2007).